ORIGINAL ARTICLE

The prognostic marker elastin correlates with epithelial–mesenchymal transition and vimentin–positive fibroblasts in gastric cancer

Tianyi Fang[1†] 🆔, Lei Zhang[2†], Xin Yin[1†], Yufei Wang[1], Xinghai Zhang[2], Xiulan Bian[2], Xinju Jiang[2], Shuo Yang[2] and Yingwei Xue[1]*

[1]Department of Gastroenterological Surgery, Harbin Medical University Cancer Hospital, Harbin Medical University, Harbin, PR China
[2]Department of Pathology, Harbin Medical University, Harbin, PR China

*Correspondence to: Yingwei Xue, Department of Gastrointestinal Surgery, Harbin Medical University Cancer Hospital, Harbin Medical University, Harbin 150081, China. E-mail: xueyingwei@hrbmu.edu.cn

[†]These authors contributed equally to this work.

Abstract

Elastin (ELN) fibers are essential constituents of the tumor microenvironment of gastric cancer (GC). However, few studies have investigated the clinical prognostic significance of ELN in GC. We screened for molecular markers that were highly related to distant metastasis by transcriptome sequencing. The Cancer Genome Atlas (TCGA) and Harbin Medical University (HMU) validation cohorts were used to validate ELN expression and to explore molecular mechanisms. Immunohistochemistry for ELN, vimentin (VIM), and fibroblast activation protein, and elastic fiber–specific staining were used to evaluate the relationship between ELN and prognosis. R studio was used to construct a nomogram prognostic model. In this study, we found that *ELN* mRNA levels were significantly higher in cancer tissues and were associated with poor prognosis in TCGA and HMU patients. Gene set enrichment analysis showed that ELN was mainly enriched in the epithelial–mesenchymal transition (EMT) pathway. The mRNA expression of *ELN* was positively correlated with fibroblast molecular markers, especially *VIM*. For validation, we collected a tissue microarray containing 180 pairs of samples. We found that ELN was positively correlated with VIM expression in cancer tissue but not in paracancerous tissues by immunohistochemistry staining. Univariate and multivariate analyses showed that the expression of ELN and lymph node metastasis rate were independent predictors for overall survival. Moreover, a nomogram model was used to evaluate the risk of death by combining the expression of *ELN* and lymph node metastasis rate. ELN may play an important role in the progression of GC by regulating EMT and is a useful prognostic indicator in predicting the prognosis of GC.

Keywords: gastric cancer; ELN; EMT; fibroblast; prognosis

Introduction

Gastric cancer (GC) is still a leading cause of cancer death in East Asia, Eastern Europe, and South America, and it results in more than 700,000 deaths per year [1]. More than 70% of the new cases and deaths occur in developing countries and regions, and thus, GC has caused a social burden that cannot be ignored. In most developing countries, the early diagnosis rate of GC remains low, approximately 6–19%. However, in developed countries, such as Japan, South Korea, and America, the detection rate of early GC can be greater than 50% [2–4]. Moreover, the prognosis of GC is closely related to the timing of treatment, and most early GC cases can be treated with radical treatment. However, even if metastatic GC is treated with surgery, the 5-year survival rate is still less than 10% [5–7]. At present, it is believed that the most common routes of metastasis are lymph node metastasis, direct invasion, and hematogenous spread. Hematogenous metastasis is the most malignant form of GC metastasis [8–10]. Therefore, biomarkers for the early evaluation of blood-borne metastasis and the development therapeutic targets for the treatment of GC are urgently needed.

Tumor cells, cancer-associated fibroblasts (CAFs), surrounding tissues, immune cells, blood vessels, extracellular matrix, and other elements form the tumor microenvironment (TME) [11,12]. CAFs interact with the extracellular matrix to promote tumor development and metastasis. Communication between tumor cells and CAFs has been extensively studied. Fibroblasts can activate a misguided wound-healing response while recruiting immune cells and affecting vascular permeability [13,14]. Moreover, CAFs can secrete a large amount of oncogenic elastin (ELN) to promote tumor proliferation and metastasis [15,16]. Recently, it has been reported that the extracellular matrix of dormant tumors is mainly composed of coiled and disorganized elastic fibers, while the elastic fibers of the highly active tumor extracellular matrix are straight and have more directional linear arrangements [17]. Although a large number of stromal features associated with tumors have long been recognized, the establishment of reliable biomarkers for such stromal features requires further investigation. The ability of CAFs and ELN to further support and suppress GC tumors may be helpful for the development of effective therapeutic methods.

In this study, we attempted to analyze the high correlation between ELN and distant metastasis by transcriptomic analysis of distant metastatic and non-distant metastatic cancer tissues and paracancerous control tissues. Through bioinformatic analysis, we further explored the molecular functional mechanism of ELN. Finally, 180 patients with GC who underwent radical surgery at the Cancer Hospital of Harbin Medical University were randomly selected. H&E staining and immunohistochemistry of tissue microarray (TMA) were used to explore the relationship between ELN and CAFs. The clinicopathological factors and expression level of ELN were analyzed to construct a nomogram to predict prognosis.

Materials and methods

Overview of the GC RNA dataset and immunohistochemical GC cohort

The training cohort included 6 distant metastatic GC patients with M1 stage disease and 36 non-distant metastatic GC patients with M0 stage disease. The validation set consisted of 246 fresh frozen tumor specimens and paracancerous specimens. Clinical data from patients with GC who underwent gastrectomy as their primary treatment at Harbin Medical University Cancer Hospital were used to construct the HMU-GC validation cohort (GSE184336 and GSE179252). All samples were collected from patients after obtaining written informed consent. RNA isolation, library construction, and mRNA sequencing were performed by Novogene Biotech Co., Ltd. (Beijing, China). The data were deposited in the Gene Expression Omnibus repository. The study was approved by the Harbin Medical University Cancer Hospital Institutional Review Board.

The clinical samples for preparation of the TMA included 180 patients who underwent radical gastrectomy in the Department of Gastrointestinal Surgery, Harbin Medical University Cancer Hospital between November 2018 and December 2019.

Preparation of TMAs

The TMAs were made from the cancer tissues and paracancerous tissues of these 180 patients. Due to the heterogeneity of tumor cells, whether a 1.5 mm diameter sample on a tissue chip can fully represent the original tissue specimen is controversial. Therefore, two experienced pathologists observed the pathological level of the entire tumor tissue by H&E staining under a high-definition microscope, and selected a representative location to more accurately reflect the pathological characteristics of the tumor.

For paracancerous tissue (normal tissues), we ensured that the sampling site was at least 5 cm away from the visible tumor, and confirmed that there was no tumor tissue by H&E staining. We marked the selected points with a special marker on the paraffin block. The technical service was provided by Shanghai Outdo Biotech Co., Ltd. (Shanghai, China).

Statistical analyses and bioinformatics analyses

Overall survival (OS) was defined as the time from surgery to death due to GC. If patients were alive at the last follow-up, they were censored. Categorical data were tested using Mann–Whitney and Fisher's exact tests for continuous data. The chi-squared test was used to analyze the association between mRNA expression, immunohistochemical expression levels, and clinicopathological characteristics. The log-rank test and Kaplan–Meier analysis were used to analyze the survival curves. Hazard ratios and 95% CIs were estimated by Cox regression models. Pearson correlation analysis was conducted to test the correlation between two continuous correlated variables. Gene Ontology (GO) pathway enrichment analysis was used for genome functional annotation. The functional enrichment of risk score-associated genes was investigated in gene set enrichment analysis (GSEA) using the 'ClusterProfiler' package. ESTIMATE

(https://bioinformatics.mdanderson.org/estimate) was used to analyze tumor purity, the level of stromal cells, and the infiltration level of immune cells in each GC sample across TCGA. All bioinformatics analyses were performed using R Studio software (v4.0.2). For all statistical analyses, SPSS 22.0 (IBM Corp., Armonk, NY, USA) was used. Two-tailed P values <0.05 were considered significant.

Immunohistochemistry and immunohistochemistry assessment

Sections from the TMA were placed in a 65 °C oven for 2 h. After immersion in xylene solution for 30 min, the TMA sections were dehydrated in a tissue gradient as follows: absolute ethanol for 5 min, 95% ethanol for 5 min, 85% ethanol for 5 min, and a water rinse for 5 min. Sections were washed three times in PBS for 5 min. Antigen retrieval was performed with sodium citrate, pH 6.0, at 120 °C for 3 min, followed by washing three times in PBS. Endogenous peroxidase was removed by 3% hydrogen peroxide for 30 min, and then goat serum was added to block for 1 h. The diluted primary antibody (ELN: 1:200, A12433, ABclonal Technology, Wuhan, China; vimentin [VIM]: 1:200, A19607, ABclonal Technology) was added, and the histochemical cartridge was placed in a refrigerator at 4 °C overnight. VIM is known to be a nonspecific parameter in histological analysis especially for fibroblasts. In order to specifically screen VIM positive fibroblasts, we also performed staining for fibroblast activation protein (FAP) (1:150, ab207178, Abcam, Cambridge, UK) staining to determine the expression position of fibroblasts. The next day, the histochemical cassette was placed in a 37 °C incubator for 45 min, and then washed in PBS. After the secondary antibody was added dropwise, the tissue array was placed in a 37 °C incubator for 40 min. The chromogenic reaction was performed via DAB staining. Finally, hematoxylin was used for nuclear staining. All specimens were reviewed by two independent blinded pathologists based on the extent of positively stained cells.

For immunohistochemistry assessment, the TMA was scanned using the Leica pathology microscope DM4B (Leica Microsystems GmbH, Wetzlar, Germany) and viewed at ×200 total magnification for evaluation. The tumor stroma staining was assessed using a semiquantitative immunohistochemical H-score (0–300), which was derived from the staining intensity, scored as negative (0), weak (1), medium (2), or strong (3), multiplied by the area percentage of staining under that intensity. Both ELN and VIM-positive fibroblasts showed staining in the tumor stroma. The immunohistochemistry scores were stratified into high expression or low expression based on survival using X-tile software.

Elastic fiber staining on paraffin–embedded slides

The methods of dewaxing and dehydration for TMA were as described above. Then, the TMAs were soaked in oxalic acid solution for 5 min at room temperature and washed three times with PBS. The slides were soaked in 95% ethanol for 30 s, and ELN solution was added at 4 °C overnight (prepared according to the following protocol: basic fuchsin 1 g, resorcin 2 g, distilled water 100 ml, 30% ferric chloride 12.5 ml, and concentrated hydrochloric acid 2 ml. First, add basic fuchsin, resorcinol, and distilled water into the beaker and boil. Slowly add ferric chloride, boil for 3 min, then cool and filter. Dry the filtered crystals, add 100 ml absolute ethanol and dissolve it in a 80 °C water bath. After cooling, add concentrated hydrochloric acid). The next day, TMAs were first soaked in 95% ethanol for 2 min and then counterstained in Van Gieson's solution for 1 min. The TMAs were washed three times in PBS solution and then dehydrated. Then, they were soaked in xylene solution and finally mounted and observed under a microscope. Elastic fibers are stained blue–black, cancer cells are stained yellow, and muscle fibers are stained red [18].
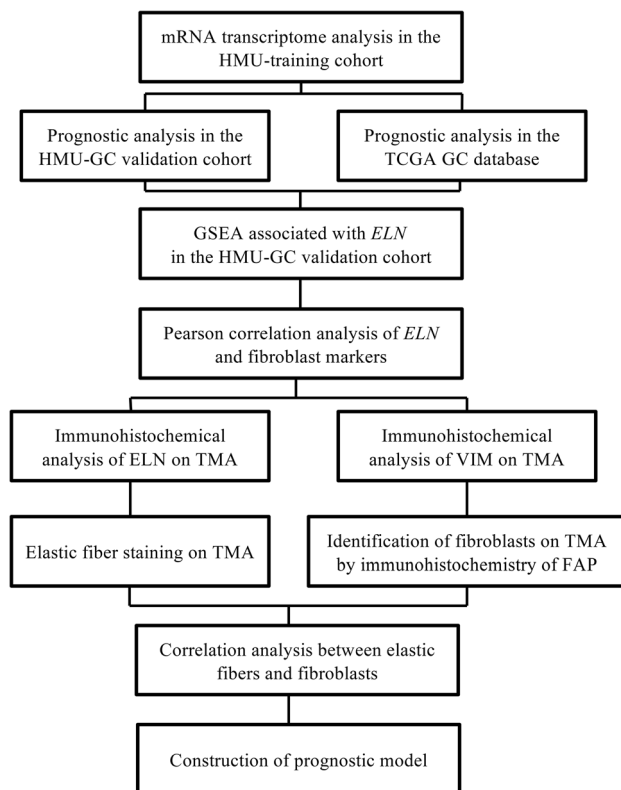
Results

Expression of ELN in GC in the training cohort

The workflow chart of the study design is shown in Figure 1. Genes associated with distant metastasis of GC were screened by mRNA transcriptome sequencing technology. The clinicopathological characteristics of 6 distant and 36 non-distant metastases in the HMU-training cohort were not significantly different by the chi-squared test (supplementary material, Table S1). We found that ELN was highly expressed in GC tissues with distant metastasis, and the mRNA expression was 2.91-fold higher than that in GC tissues with non-distant metastasis (Figure 2A).

ELN plays an oncogenic role in GC, and high ELN mRNA expression predicts poor prognosis

To explore the expression level and prognostic role of ELN in GC, we analyzed the RNA-seq dataset and the corresponding clinical characteristics from the Harbin Medical University Cancer Hospital validation cohort and TCGA GC database. ELN was found to be significantly upregulated in paired GC tissues ($N = 246$,

```
mRNA transcriptome analysis in the
HMU-training cohort
```

```
Prognostic analysis in the          Prognostic analysis in the
HMU-GC validation cohort            TCGA GC database
```

```
GSEA associated with ELN
in the HMU-GC validation cohort
```

```
Pearson correlation analysis of ELN
and fibroblast markers
```

```
Immunohistochemical              Immunohistochemical
analysis of ELN on TMA           analysis of VIM on TMA
```

```
Elastic fiber staining on TMA    Identification of fibroblasts on TMA
                                 by immunohistochemistry of FAP
```

```
Correlation analysis between elastic
fibers and fibroblasts
```

```
Construction of prognostic model
```

Figure 1. The study protocol was designed and performed according to the declaration of Helsinki and was approved by the local ethics committee.

$p < 0.001$; $N = 32$, $p < 0.05$) compared to normal tissues. We obtained the same results when comparing all GC tissues and normal tissues ($p < 0.001$, $p < 0.01$; Figure 2B, C). In the HMU-GC validation cohort and the TCGA GC dataset, GC patients with high *ELN* expression showed poorer OS probability ($p = 0.041$, $p = 0.021$; Figure 2D, E). The results suggest that *ELN* may be a prognostic marker in GC patients. In general, patients with stage IV have a poor prognosis, while patients with stage I have a better prognosis. Therefore, this study further analyzed the relationship between *ELN* expression and prognosis in patients with GC in the intermediate stages (stages II and III). GC patients with higher *ELN* expression also showed poorer OS probability ($p = 0.058$, $p = 0.062$, close to being significant; Figure 2F,G).

Relationship between *ELN* expression and the clinical characteristics of GC

We first analyzed the stromal score and tumor purity of TCGA GC patients according to the expression level of *ELN* to estimate whether the proportion of neoplastic cell

to non-neoplastic cell in the tumor tissue is related to the expression of *ELN*. Stromal score ($p < 0.0001$), immune score ($p < 0.001$), and ESTIMATE score ($p < 0.0001$) were significantly increased in the *ELN* over-expression group (Figure 2H). However, the *ELN* over-expression group showed lower tumor purity (tumor purity = cos $(0.6049872018 + 0.0001467884 \times$ ESTIMATE score)) ($p < 0.0001$; Figure 2I). To explore the relationship between *ELN* expression and the clinical characteristics of GC, we analyzed the expression of *ELN* in the HMU-GC validation cohort. The results showed that *ELN* expression was significantly correlated with T classification, N classification, and TNM classification (Table 1). Moreover, *ELN* expression was significantly upregulated in the T3 + T4 group ($p < 0.05$; Figure 2J), N2 + N3 group ($p < 0.05$; Figure 2K), TNM II + III + IV group ($p < 0.01$; Figure 2L), and worse histological type group ($p < 0.05$; Figure 2M). These results show that high *ELN* expression is associated with GC progression.

ELN regulates GC progression through the EMT pathway

To clarify the underlying mechanism by which *ELN* acts in GC progression, we performed GSEA based on high *ELN* expression and low *ELN* expression groups in the HMU-GC validation set. The HALLMARK epithelial–mesenchymal transition (EMT) pathway was the most enriched gene signature (Figure 3A). In addition, Pearson correlation test analysis revealed that *ELN* was negatively correlated with *E-CAD* expression. Other EMT classic signatures, including *N-CAD*, SNAIL (*SNAI1*), SLUG (*SNAI2*), *TWIST1*, and *TWIST2*, showed a significant correlation with *ELN* (Figure 3B). Moreover, the TGF-β signaling pathway and the WNT-β-Catenin signaling pathway were significantly enriched (Figure 3C). These findings suggest that ELN may promote GC progression by regulating the EMT pathway. GO analysis showed that ELN mainly affects the synthetic function of organelles within the cytoplasm in terms of cellular components. In terms of molecular function, it mainly affects the binding of cytoskeletal proteins and actin. Biological processes mainly affect anatomical structure morphogenesis, such as vasculature development and cellular component organization or biogenesis (Figure 3D–G).

The mRNA level of *ELN* is highly correlated with fibroblast markers

The literature indicates that ELN is mainly secreted by fibroblasts in the TME. To explore the relationship between *ELN* expression and fibroblasts, a heatmap of
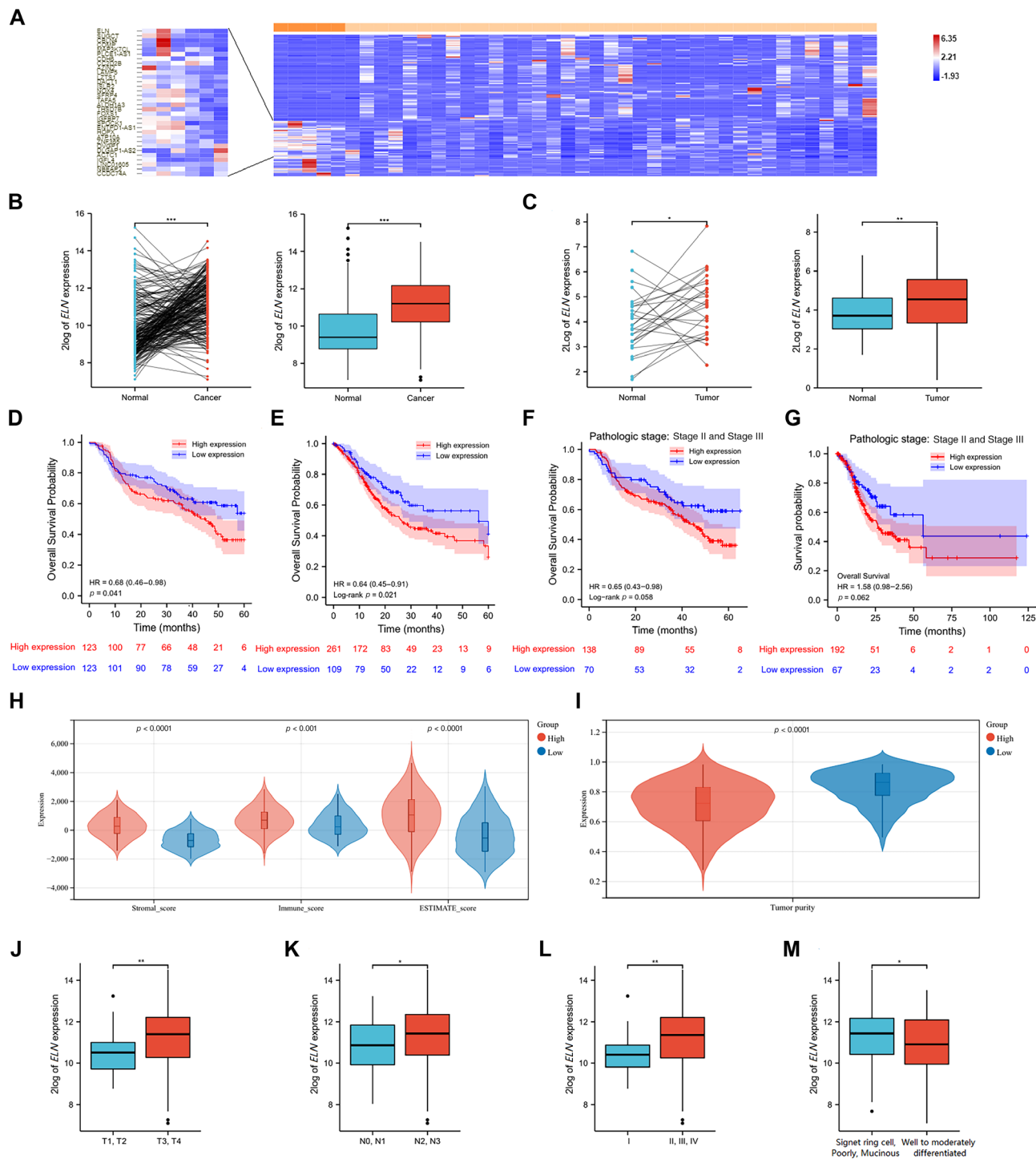
Figure 2. (A) Heatmap showing genes associated with distant metastasis of gastric cancer. (B) The expression of *ELN* in paired GC samples and all GC samples from HMU–GC validation cohort. (C) The expression of *ELN* in paired GC samples and all GC samples from TCGA. (D) Kaplan–Meier survival analysis of the OS for patients with different *ELN* expression in the HMU–GC validation cohort. (E) Kaplan–Meier survival analysis of the OS for patients with different *ELN* expression in TCGA. (F) Kaplan–Meier survival analysis of the OS for stage II and III patients in the HMU–GC validation cohort. (G) Kaplan–Meier survival analysis of the OS for stage II and III patients in TCGA. (H) Stromal score, immune score, and ESTIMATE score were significantly increased in the *ELN* over-expression group. (I) The *ELN* over-expression group showed lower tumor purity. *ELN* expression was associated with the clinicopathological characteristics of GC in the HMU–GC validation cohort. (J) T classification, (K) N classification, (L) pTNM classification, and (M) WHO classification.

the correlations among *ELN* fibroblast surface markers, including *CAV1*, *VIM*, *S100A4*, *FAP*, and *PDPN*, was generated ($p < 0.05$; Figure 4A). In addition, the expression of *ELN* and the fibroblast surface markers *CAV1* ($r = 0.653$, $p < 0.001$), *VIM* ($r = 0.684$, $p < 0.001$), *S100A4* ($r = 0.377$, $p < 0.001$), *FAP* ($r = 0.570$, $p < 0.001$), and *PDPN* ($r = 0.377$, $p < 0.384$) was significantly positively correlated, and *VIM* had the strongest correlation (Figure 4B).

ELN and VIM–positive fibroblast expression in clinical samples

To further explore the expression patterns of ELN and VIM-positive fibroblasts in GC clinical samples, TMA immunohistochemistry staining was performed in 180 pairs of primary tumor tissues and paracancerous control tissues. As shown in Figure 5A–D, ELN immunohistochemistry and elastin Van Gieson staining showed that ELN-positive elastin is mainly expressed in cancer interstitial fibrous tissue. VIM was widely expressed on fibroblasts in the tumor stroma and FAP was highly expressed in the fibroblasts of cancer stroma and slightly expressed in the cytoplasm of tumor cells. Meanwhile, we found that FAP was widely expressed in the stroma in poorly differentiated adenocarcinomas (Figure 5C5). In well to moderately differentiated, poorly differentiated, and mucinous adenocarcinomas, ELN was expressed in the stromal fibrous tissue of the carcinoma, in the same location as the elastic fibers, and VIM was widely expressed in the fibroblasts and tumor stroma of various pathological types. Furthermore, we found that ELN expression in cancer tissues was highly correlated with VIM expression in cancer tissues but not correlated with VIM expression in paracancerous tissues (Figure 5E). The median H-score of ELN expression in tumor stroma was 29, with a range of 0–300. The X-tile cut-point was 45 with 39.4% of patients (71/180) showing low expression and 60.6% of patients showing high expression. The median H-score of VIM-positive fibroblast in tumor stroma was 149, ranging from 0 to 300. The X-tile cut-point was 138 with 47.2% of patients (85/180) showing low expression and 52.7% of patients showing high expression.

ELN expression in cancer tissues was significantly associated with lymph node metastasis (Table 2), and ELN in paracancerous tissues was associated with Lauren classification (supplementary material, Table S2). Furthermore, VIM in cancer tissues was mainly associated with T classification, tumor invasion pattern, Lauren classification, and carcinoembryonic antigen (CEA) (Table 3) but not with clinicopathological characteristics in paracancerous tissues (supplementary material, Table S3). This may suggest that GC metastasis relying on ELN is caused by the secretion of elastic fibers from VIM-positive fibroblasts in cancer tissue.

The expression of ELN correlates with prognosis and can be used to construct a prognostic model

A total of 100 individuals reached the 3-year follow-up in our TMA, so we analyzed survival-related data in these samples. The results showed that 38 out of 100 people had positive ELN staining. We analyzed the relationship between high and low ELN expression and OS by Kaplan–Meier analysis and found that it was significantly associated with OS (Figure 6C). Univariate Cox regression analysis showed that ELN expression ($p < 0.001$) and the lymph node metastasis rate ($p < 0.001$) were prognostic risk factors (Figure 6A). Multivariate Cox regression analysis indicated that ELN expression ($p = 0.043$) and the lymph node metastasis rate ($p = 0.022$) were independent prognostic risk factors (Figure 6B). Furthermore, we constructed a prognostic model based on the results of the multivariate analysis, and this model could predict 2-year and 3-year survival (Figure 6D). Finally, we verified that the prognostic model had satisfactory predictive value by calibration curve analysis, and the calibration analysis showed that the *C*-index was 0.714 (0.669–0.759) (Figure 6E). Decision curve analysis showed that the combination of ELN expression and the lymph node metastasis rate was better than the lymph node metastasis rate at both 2 and 3 years [0.714 (0.669–0.759) versus 0.647 (0.593–0.702)] (Figure 6F).

Discussion

Fibroblasts accumulate in the TME and contribute to the emergence and progression of GC [19,20]. This not only provides abundant growth factors for stromal components of the TME and promotes the proliferation of cancer cells but also creates a suitable physical environment for lymphatic metastasis and blood metastasis of cancer cells [21–23]. In current clinical applications, CAV1, VIM, S100A4, FAP, and PDPN are all specific markers for assessing the enrichment of fibroblasts around cancer cells [24,25]. Recent studies have attempted to elucidate the key molecular mechanisms by which fibroblasts promote cancer. However, due to the extremely high heterogeneity of GC, no reliable biomarkers have been proposed for clinical application. To better understand the mechanism of

Table 1. The relationship between *ELN* mRNA expression and the clinical characteristics of GC in the HMU-GC validation cohort

Characteristic	Low expression	High expression	*P* value
Number of patients	123	123	
Age (median, IQR)	59 (48, 65.5)	57 (48.5, 65)	0.654
Sex			0.352
Male	40 (16.3%)	48 (19.5%)	
Female	83 (33.7%)	75 (30.5%)	
T classification, *n* (%)			**0.006**
T1a	3 (1.2%)	3 (1.2%)	
T1b	7 (2.8%)	0 (0%)	
T2	14 (5.7%)	3 (1.2%)	
T3	73 (29.7%)	92 (37.4%)	
T4a	16 (6.5%)	14 (5.7%)	
T4b	10 (4.1%)	11 (4.5%)	
N classification, *n* (%)			**0.015**
N0	31 (12.6%)	18 (7.3%)	
N1	18 (7.3%)	11 (4.5%)	
N2	23 (9.3%)	19 (7.7%)	
N3a	36 (14.6%)	43 (17.5%)	
N3b	15 (6.1%)	32 (13%)	
M stage, *n* (%)			0.315
M0	117 (47.6%)	112 (45.5%)	
M1	6 (2.4%)	11 (4.5%)	
pTNM, *n* (%)			**0.002**
IA	9 (3.7%)	2 (0.8%)	
IB	9 (3.7%)	1 (0.4%)	
IIA	10 (4.1%)	13 (5.3%)	
IIB	14 (5.7%)	9 (3.7%)	
IIIA	29 (11.8%)	17 (6.9%)	
IIIB	29 (11.8%)	41 (16.7%)	
IIIC	17 (6.9%)	29 (11.8%)	
IV	6 (2.4%)	11 (4.5%)	
Borrmann type, *n* (%)			0.718
Borrmann 1	3 (1.2%)	2 (0.8%)	
Borrmann 2	27 (11%)	23 (9.3%)	
Borrmann 3	75 (30.5%)	74 (30.1%)	
Borrmann 4	18 (7.3%)	24 (9.8%)	
Tumor location, *n* (%)			0.137
Lower	52 (21.1%)	66 (26.8%)	
Middle	33 (13.4%)	22 (8.9%)	
Entire stomach	13 (5.3%)	17 (6.9%)	
Unknown	25 (10.2%)	18 (7.3%)	
Lymphatic infiltration, *n* (%)			0.367
Negative	57 (23.2%)	49 (19.9%)	
Positive	66 (26.8%)	74 (30.1%)	
Nerve infiltration, *n* (%)			0.441
Negative	30 (12.2%)	24 (9.8%)	
Positive	93 (37.8%)	99 (40.2%)	
WHO classification, *n* (%)			0.162
Mucinous	5 (2%)	4 (1.6%)	
Poorly differentiated	33 (13.4%)	31 (12.6%)	
Signet ring cell	35 (14.2%)	51 (20.7%)	
Well to moderately differentiated	50 (20.3%)	37 (15%)	
CEA (median, IQR)	2.28 (1.41, 4.16)	1.86 (1.23, 3.33)	0.188
CA19-9 (median, IQR)	11.59 (6.06, 22.25)	10.58 (5.06, 23.09)	0.905
CA72-4 (median, IQR)	2.66 (1.19, 6.89)	3.03 (1.33, 7.85)	0.447
CA125 (median, IQR)	10.97 (7.84, 15.78)	9.45 (7.81, 13.41)	0.164

Histological type, T classification, N classification, and pTNM classification were according to the AJCC 8th edition of the Cancer Staging Manual of the American Joint Committee on Cancer. Vascular infiltration, nerve infiltration, and lymphatic infiltration were determined according to the postoperative pathology report. IQR, interquartile range. Statistically significant *P* values are marked in bold font.
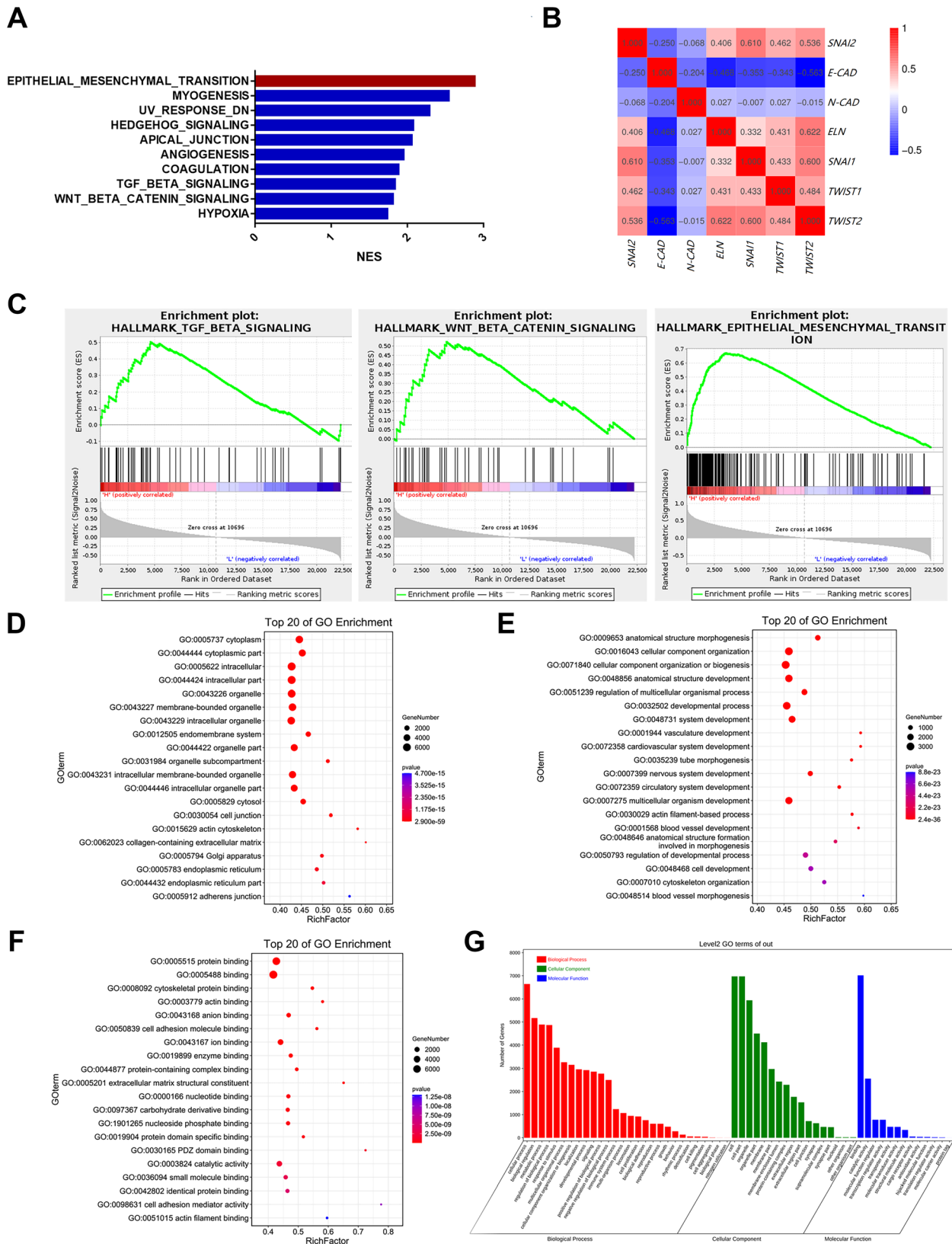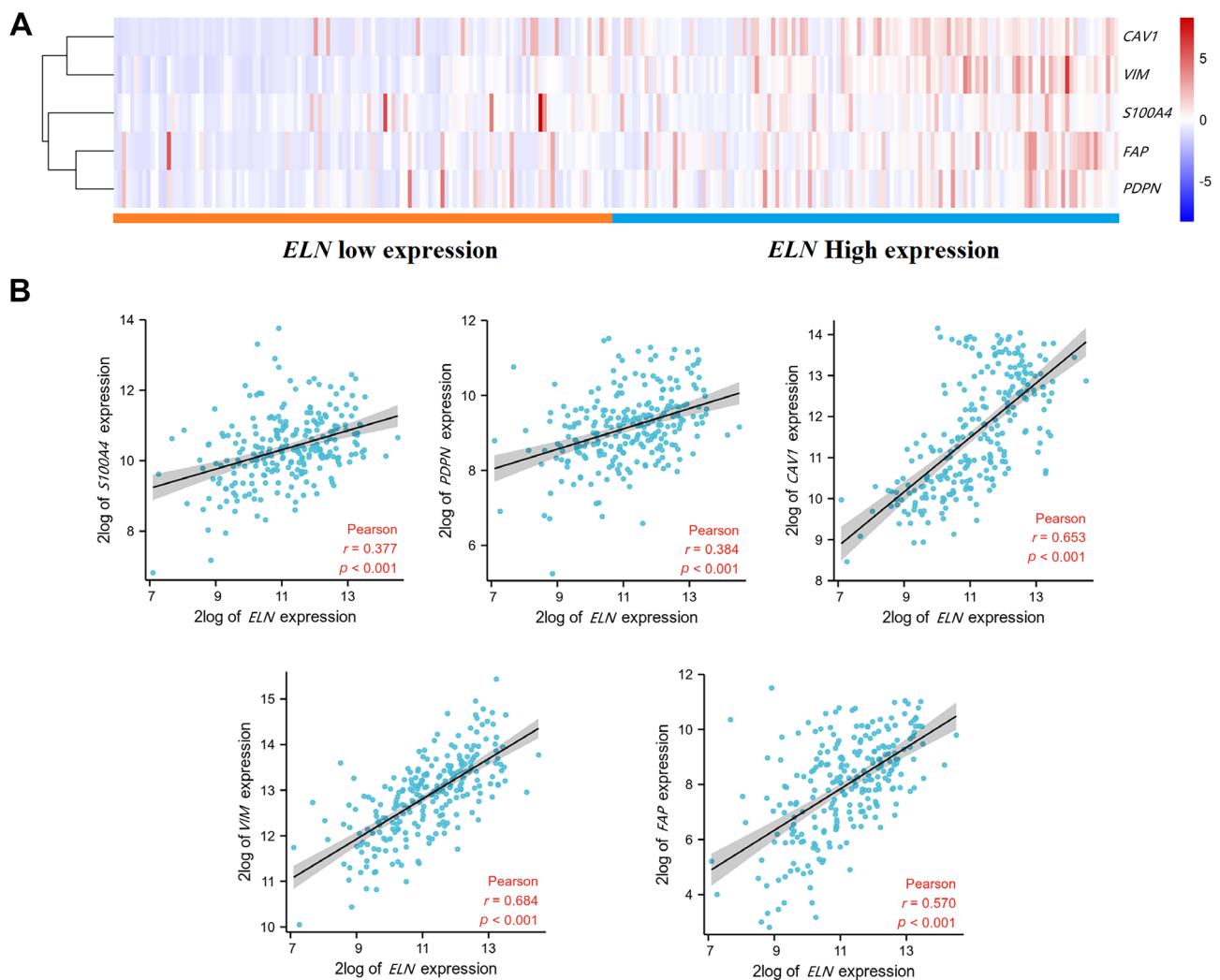
Figure 3. Legend on next page.

Figure 4. *ELN* expression was significantly associated with the markers of fibroblast expression. (A) Heatmap of markers of fibroblasts based on *ELN* expression. (B) The correlation between *ELN* expression and fibroblast markers.

GC metastasis, we found that ELN, a product of fibroblasts, was highly correlated with the pathological features of distant metastasis by bioinformatics. This study analyzed the mRNA level and immunohistochemical expression of ELN, as well as the relationship between their expression levels and clinicopathological factors in GC patients. We propose that promoting the EMT of tumor cells is the main

molecular mechanism of ELN. We further verified the close spatial association between ELN and VIM-positive fibroblasts. Finally, we constructed a 3-year prognostic model for GC.

ELN is currently believed to be a core component of elastic fibers. These fibers impart elasticity and recoil to tissues and organs and play an important role in inducing cellular biochemical responses against the

Figure 3. (A) *ELN* expression correlated with EMT signatures in GC from the HMU-GC validation cohort. (B) *ELN* expression was positively correlated with SNAIL (*SNAI1*), SLUG (*SNAI2*), N-CAD, *TWIST1*, and *TWIST2* and negatively correlated with *E-CAD*. (C) GSEA enrichment including TGF-β, WNT-β, and EMT in the HMU-GC validation cohort. (D) GO enrichment analysis of the cellular components. (E) GO enrichment analysis of the biological processes. (F) GO enrichment analysis of the molecular functions. (G) The number of differential genes in the biological processes, cellular components, and molecular functions.

ELN ×50 ELN ×400 EVG ×400 H&E ×400 VIM ×400 FAP ×400
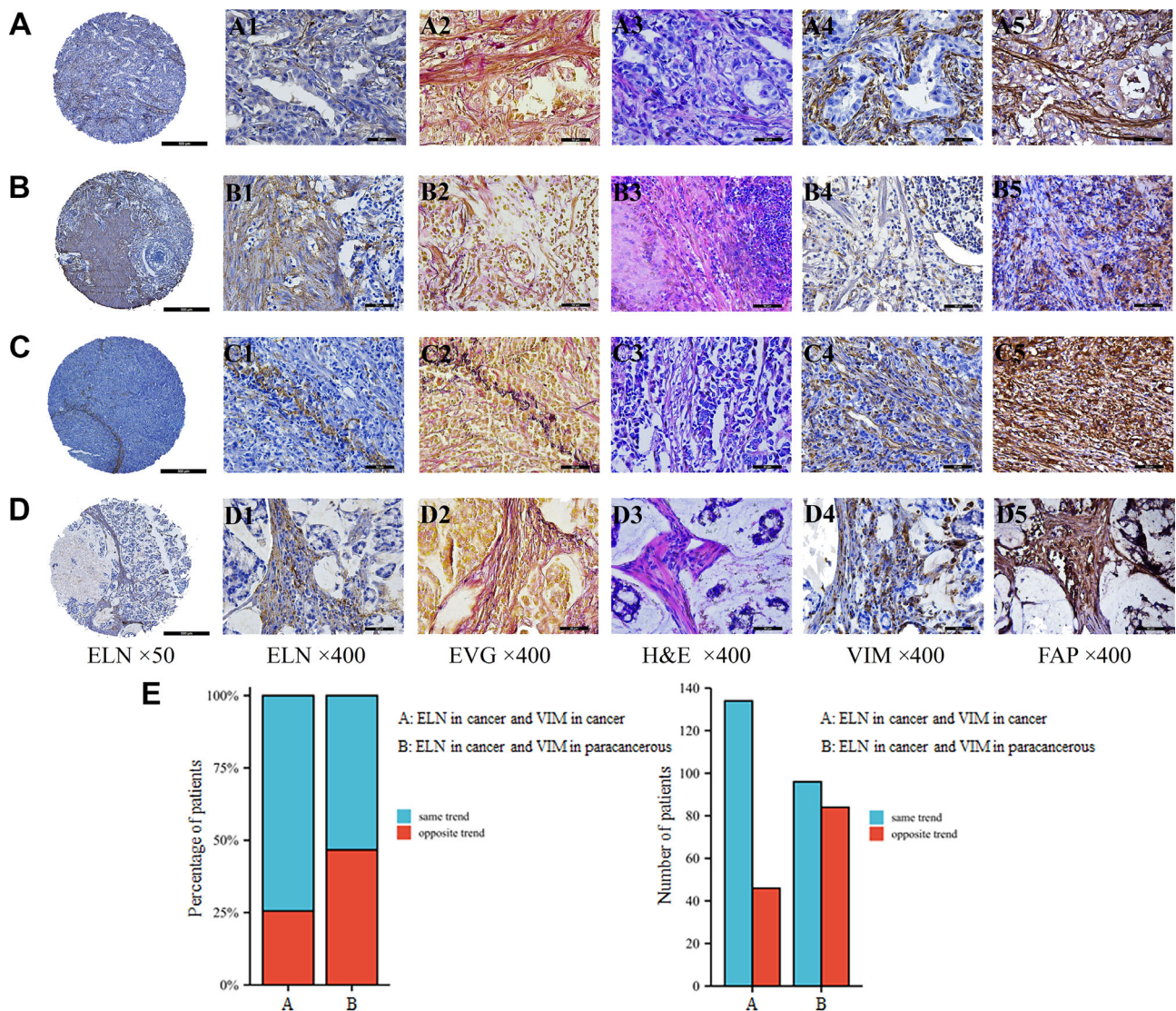
Figure 5. ELN immunohistochemistry, elastin Van Gieson (EVG) staining, H&E staining, VIM immunohistochemical staining, and FAP immunohistochemical staining of gastric cancer TMA, ×50 and ×400 total magnification. (A) Well-differentiated adenocarcinoma. (A1) ELN is mainly expressed in cancer interstitial fibrous tissue. (A2) EVG staining shows that elastic fibers are mainly expressed in cancer interstitial fibrous tissue. (A3) H&E staining shows well-differentiated adenocarcinoma and its stroma. (A4) VIM is widely expressed on fibroblasts in the tumor stroma. (A5) FAP is highly expressed in the fibroblasts of cancer stroma and slightly expressed in the cytoplasm of tumor cells. (B) Moderately differentiated adenocarcinoma, various staining, and expression positions are the same as in (A). (C) Poorly differentiated adenocarcinoma, various staining, and expression positions are the same as in (A), except for FAP. FAP is widely expressed in the tumor stroma in poorly differentiated adenocarcinoma. (D) Mucinous adenocarcinoma, various staining and expression positions are the same as in (A). H&E staining shows the pathological features of tumors with different degrees of differentiation: (A and B) intestinal-type gastric cancer, well to moderately differentiated adenocarcinoma. (C and D) poorly differentiated in diffuse-type gastric cancer and mucinous adenocarcinoma. In well to moderately differentiated, poorly differentiated, and mucinous adenocarcinomas, ELN is expressed in the stromal fibrous tissue of the tumor, in the same location as the elastic fibers. VIM is widely expressed in the fibroblasts and tumor stroma of various pathological types. FAP is also widely expressed in the fibroblasts and slightly expressed in the cytoplasm of tumor cells. (E) Correlation between ELN in cancer with VIM in cancer and VIM in paracancerous tissues.

Table 2. The relationship between ELN expression in tumor tissue and clinicopathological characteristics

Characteristic	ELN high expression	ELN low expression	P value
Number of patients	71	109	
Age (mean ± SD)	60.15 ± 8.36	60.34 ± 10.13	0.894
BMI (median, IQR)	22.99 (21.02, 24.89)	22.84 (20.38, 24.98)	0.641
Sex, n (%)			0.565
Female	16 (8.9%)	30 (16.7%)	
Male	55 (30.6%)	79 (43.9%)	
Tumor infiltration pattern, n (%)			0.081
INFa	11 (6.1%)	25 (13.9%)	
INFb	15 (8.3%)	29 (16.1%)	
INFc	35 (19.4%)	33 (18.3%)	
N/A	10 (5.6%)	22 (12.2%)	
Lymphatic infiltration, n (%)			0.078
Negative	34 (18.9%)	68 (37.8%)	
Positive	37 (20.6%)	41 (22.8%)	
Venous infiltration, n (%)			0.219
Negative	48 (26.7%)	84 (46.7%)	
Positive	23 (12.8%)	25 (13.9%)	
Nerve infiltration, n (%)			0.718
Negative	17 (9.4%)	30 (16.7%)	
Positive	54 (30%)	79 (43.9%)	
T classification, n (%)			0.121
T1	2 (1.1%)	8 (4.4%)	
T2	7 (3.9%)	20 (11.1%)	
T3	26 (14.4%)	42 (23.3%)	
T4	36 (20%)	39 (21.7%)	
N classification, n (%)			0.002
N0	15 (8.3%)	35 (19.4%)	
N1	7 (3.9%)	29 (16.1%)	
N2	20 (11.1%)	21 (11.7%)	
N3	29 (16.1%)	24 (13.3%)	
pTNM stage, n (%)			0.003
I	6 (3.3%)	17 (9.4%)	
II	14 (7.8%)	42 (23.3%)	
III	51 (28.3%)	50 (27.8%)	
Metastatic lymph node ratio, n (%)			<0.001
<0.3	45 (25%)	95 (52.8%)	
≥0.6	7 (3.9%)	5 (2.8%)	
≥0.3, <0.6	19 (10.6%)	9 (5%)	
Borrmann type, n (%)			0.616
Borrmann 1	6 (3.3%)	9 (5%)	
Borrmann 2	16 (8.9%)	33 (18.3%)	
Borrmann 3	41 (22.8%)	59 (32.8%)	
Borrmann 4	8 (4.4%)	8 (4.4%)	
Lauren classification, n (%)			0.626
Diffuse	29 (16.1%)	35 (19.4%)	
Intestinal	18 (10%)	31 (17.2%)	
Mixed	14 (7.8%)	22 (12.2%)	
Unknown	10 (5.6%)	21 (11.7%)	
Family genetic history, n (%)			1.000
No	64 (35.6%)	99 (55%)	
Yes	7 (3.9%)	10 (5.6%)	
Tumor location, n (%)			0.058
Entire stomach	5 (2.8%)	1 (0.6%)	
Lower third	34 (18.9%)	63 (35%)	
Middle and upper third	32 (17.8%)	45 (25%)	
HER2 expression, n (%)			0.109
Negative	57 (31.7%)	98 (54.4%)	
Positive	14 (7.8%)	11 (6.1%)	

(Continues)

Table 2. Continued

Characteristic	ELN high expression	ELN low expression	*P* value
CEA, *n* (%)			0.473
>5 ng/ml	7 (3.9%)	16 (8.9%)	
≤5 ng/ml	64 (35.6%)	93 (51.7%)	
CA19-9, *n* (%)			0.934
>37 U/ml	8 (4.4%)	14 (7.8%)	
≤37 U/ml	63 (35%)	95 (52.8%)	
CA72-4, *n* (%)			0.989
>6 U/ml	18 (10%)	29 (16.1%)	
≤6 U/ml	53 (29.4%)	80 (44.4%)	

Histological type, T classification, N classification, and pTNM classification were according to the AJCC 8th edition of the Cancer Staging Manual of the American Joint Committee on Cancer. Vascular infiltration, nerve infiltration, and lymphatic infiltration were determined according to the postoperative pathology report. Lauren classification is based on the histology, morphology, and biological characteristics of GC.

IQR, interquartile range. Statistically significant *P* values are marked in bold font.

mechanical forces of the microenvironment [26,27]. Therefore, there is a large amount of ELN in the organs that are often deformed by force, such as the lungs, aorta and skin, and the gastrointestinal tract to maintain the physiological functions of these organs. It has been reported that ELN has a long half-life of 40–80 years [28,29]. Studies have indicated that aging and tumors can cause abnormal or broken ELN. This results in the accumulation of elastic fiber fragments, which leads to further deterioration of the disease [30,31]. In this study, we first found that the mRNA expression of *ELN* was higher in cancer tissues and was highly correlated with T classification, N classification, and TNM stage. In addition, it was found that the expression of *ELN* was increased in patients with worse biological tumor behavior, suggesting that it may be a potential biomarker for prognosis. Survival analysis found that *ELN* had satisfactory predictive prognostic value in both the HMU-GC validation cohort and TCGA patients. To verify the biomarker reliability of *ELN*, we found that *ELN* mainly regulates the EMT of tumor cells through GSEA and GO enrichment analysis. In addition to the abovementioned roles, elastic fibers are also involved in the regulation of intercellular signaling. These fibers can support aortic wall homeostasis or exert deleterious effects by modulating the TGF-β/Smad signaling pathway, which is partially similar to our results [32]. ELN may also regulate the stability of the surrounding stroma in GC through a similar signaling pathway. GO analysis revealed that *ELN* and its related genes have important roles in cytoskeletal proteins, organelle formation, and vasculature development. ELN can promote the excessive formation of microvessels and lymphatic vessels in the TME, providing physical conditions for metastasis. Debret *et al* [33] indicated that ELN can lead to the upregulation of the mRNA and protein levels of IL-1β. IL-1β is a pleiotropic cytokine that exacerbates invasiveness, adhesion, angiogenesis, and metastatic spread during melanoma progression. This is similar to the results of our bioinformatics analysis.

The physiological functions of fibroblasts include the synthesis and secretion of collagen, ELN, and proteoglycans. These secreted proteins are the raw material for collagen fibers, elastic fibers, and reticular fibers, as well as matrix components [34]. We further found that ELN in GC tissue is also highly related to fibroblasts and is most closely related to VIM. This finding is crucial for us to further study which type of fibroblasts is more involved in tumor metastasis. Ligorio *et al* [35] reported that CAFs can activate the MAPK and STAT3 signaling pathways by secreting TGF-β, etc, affecting EMT in pancreatic ductal carcinoma. This study also found that ELN secreted by fibroblasts also plays a role in regulating EMT and the activation of the TGF-β signaling pathway in GC, which also indicates the functional universality of CAFs and ELN. Through immunohistochemical and elastic fiber staining, we found that ELN in cancer tissues was mainly highly correlated with VIM. However, it was not associated with VIM expression in paracancerous tissue, which was similar to our findings at the transcriptome level. The analysis of tumor purity suggested that the proportion of tumor stroma in the tissues of patients with high expression of ELN is higher, while the proportion of tumor cells is lower. On the other hand, it also shows that ELN is more distributed in the areas with high stroma abundance. In addition, we also found that there were more VIM-fibroblasts in the diffuse GC tumor tissues, while there were fewer VIM-fibroblasts in the intestinal GC tissues. This is related to the histological characteristics of different Laurent classifications. Diffuse GC is often accompanied by a large amount of fibrous tissue

Table 3. The relationship between VIM expression in cancer tissues and clinicopathological characteristics

Characteristic	VIM high expression	VIM low expression	P value
Number of patients	85	95	
Age (mean ± SD)	60.76 ± 8.98	59.82 ± 9.87	0.505
BMI (median, IQR)	23.11 (21.16, 25.47)	22.84 (20.31, 24.53)	0.387
Sex, n (%)			1.000
Female	22 (12.2%)	24 (13.3%)	
Male	63 (35%)	71 (39.4%)	
Tumor infiltration pattern, n (%)			0.004
INFa	14 (7.8%)	22 (12.2%)	
INFb	21 (11.7%)	23 (12.8%)	
INFc	42 (23.3%)	26 (14.4%)	
N/A	8 (4.4%)	24 (13.3%)	
Lymphatic infiltration, n (%)			0.616
Negative	46 (25.6%)	56 (31.1%)	
Positive	39 (21.7%)	39 (21.7%)	
Venous infiltration, n (%)			0.778
Negative	61 (33.9%)	71 (39.4%)	
Positive	24 (13.3%)	24 (13.3%)	
Nerve infiltration, n (%)			0.111
Negative	17 (9.4%)	30 (16.7%)	
Positive	68 (37.8%)	65 (36.1%)	
T classification, n (%)			0.001
T1	4 (2.2%)	6 (3.3%)	
T2	4 (2.2%)	23 (12.8%)	
T3	38 (21.1%)	30 (16.7%)	
T4	39 (21.7%)	36 (20%)	
N classification, n (%)			0.939
N0	22 (12.2%)	28 (15.6%)	
N1	18 (10%)	18 (10%)	
N2	19 (10.6%)	22 (12.2%)	
N3	26 (14.4%)	27 (15%)	
pTNM stage, n (%)			0.094
I	6 (3.3%)	17 (9.4%)	
II	28 (15.6%)	28 (15.6%)	
III	51 (28.3%)	50 (27.8%)	
Metastatic lymph node ratio, n (%)			0.277
<0.3	62 (34.4%)	78 (43.3%)	
≥0.6	6 (3.3%)	6 (3.3%)	
≥0.3, <0.6	17 (9.4%)	11 (6.1%)	
Borrmann type, n (%)			0.338
Borrmann 1	5 (2.8%)	10 (5.6%)	
Borrmann 2	28 (15.6%)	21 (11.7%)	
Borrmann 3	45 (25%)	55 (30.6%)	
Borrmann 4	7 (3.9%)	9 (5%)	
Lauren classification, n (%)			0.019
Diffuse	38 (21.1%)	26 (14.4%)	
Intestinal	21 (11.7%)	28 (15.6%)	
Mixed	18 (10%)	18 (10%)	
Unknown	8 (4.4%)	23 (12.8%)	
Family genetic history, n (%)			0.809
No	76 (42.2%)	87 (48.3%)	
Yes	9 (5%)	8 (4.4%)	
Tumor location, n (%)			0.072
Entire stomach	1 (0.6%)	5 (2.8%)	
Lower third	41 (22.8%)	56 (31.1%)	
Middle and upper third	43 (23.9%)	34 (18.9%)	
HER2 expression, n (%)			0.895
Negative	74 (41.1%)	81 (45%)	
Positive	11 (6.1%)	14 (7.8%)	

(Continues)

Table 3. Continued

Characteristic	VIM high expression	VIM low expression	P value
CEA, n (%)			0.038
>5 ng/ml	16 (8.9%)	7 (3.9%)	
≤5 ng/ml	69 (38.3%)	88 (48.9%)	
CA19-9, n (%)			0.389
>37 U/ml	8 (4.4%)	14 (7.8%)	
≤37 U/ml	77 (42.8%)	81 (45%)	
CA72-4, n (%)			0.917
>6 U/ml	23 (12.8%)	24 (13.3%)	
≤6 U/ml	62 (34.4%)	71 (39.4%)	

Histological type, T classification, N classification, and pTNM classification were according to the AJCC 8th edition of the Cancer Staging Manual of the American Joint Committee on Cancer. Vascular infiltration, nerve infiltration, and lymphatic infiltration were determined according to the postoperative pathology report. Lauren classification is based on the histology, morphology, and biological characteristics of GC.
IQR, interquartile range. Statistically significant P values are marked in bold font.

hyperplasia, which will also include more fibroblasts. It has been reported that ELN promotes the activity of fibroblast MMP-2 in the TME, stimulates fibroblast chemotaxis, leads to the overexpression of MMP-1 and -3, and accelerates tumor angiogenesis [36]. Whether ELN or fibroblasts play the leading role in GC needs to be confirmed in further experiments.
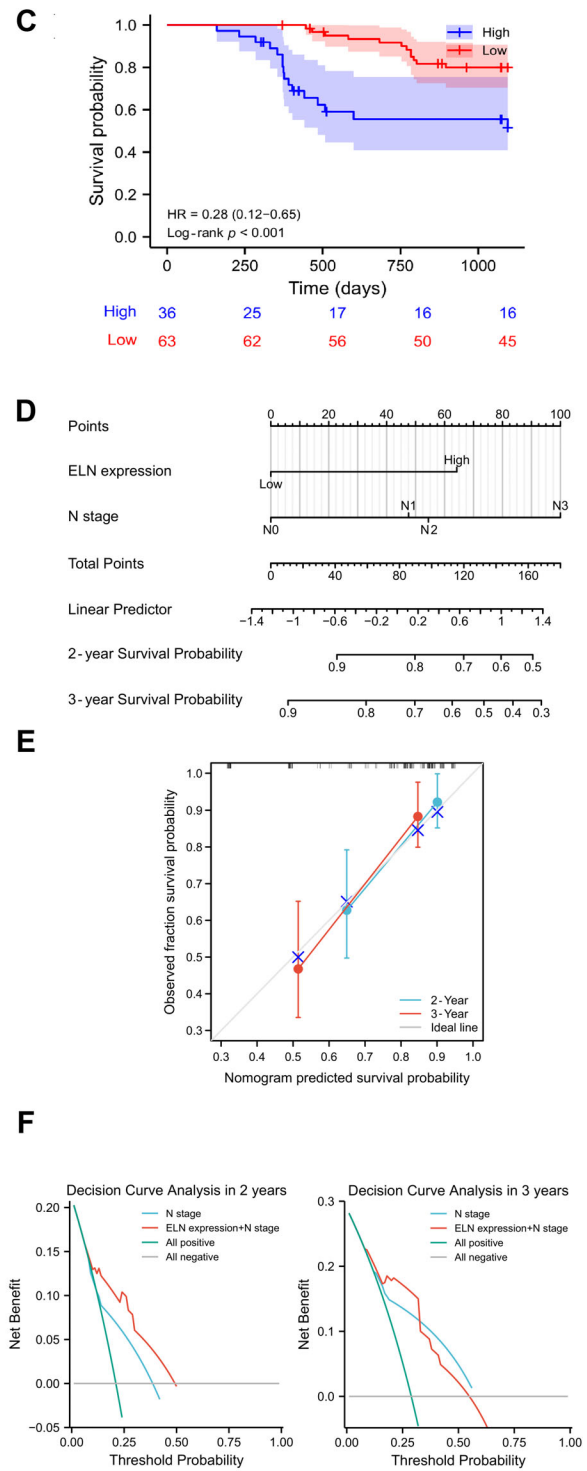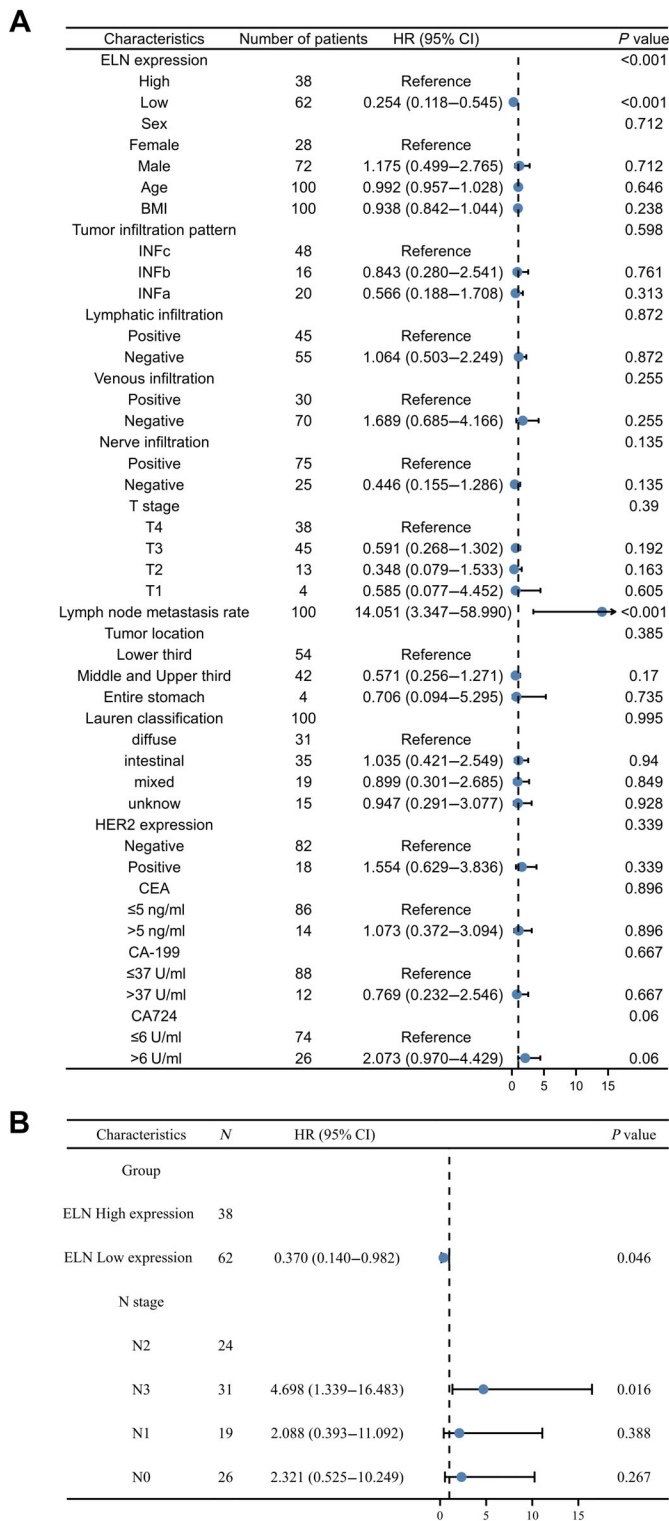
Combining ELN immunohistochemical expression with other clinicopathological characteristics for multivariate analysis, we found that ELN expression and the lymph node metastasis rate were independent prognostic factors, and patients with a higher lymph node metastasis rate or high ELN expression had poorer survival. It is well known that inflammation, angiogenesis, vascular permeability, and lymphangiogenesis are important pathological changes for tumor metastasis. In the last century, ELN has been reported to induce local inflammatory responses and adventitial angiogenesis [37]. Robinet et al [38] showed that ELN leads to the upregulation of pro-MT1-MMP and pro-MMP-2 to trigger neovascularization in their study of atherosclerosis. Gunda et al [39] further showed that this angiogenic potential can be inhibited by collagen type IV fragments, indicating the potential for the treatment of angiogenesis-dependent tumor metastases. Moreover, we observed that in patients with Lauren classification of diffuse type, their paracancerous tissue contained more ELNs. The literature points out that diffuse GC is more prone to distant metastasis [40], which is similar to the conclusion of our study. ELN in paracancerous tissues of most patients with diffuse GC may play a key role in EMT, which also plays an indispensable role in maintaining this biological behavior, more prone to distant metastasis.

With the deepening of the research on ELN for 40 years, researchers realized that the repair of ELN may be a means to prevent tumor metastasis [17,41,42].

However, due to its hydrophobicity and extensive cross-linking, ELN in the extracellular matrix is insoluble and highly resistant to other proteins. ELN causes damage associated with aging and disease, which may lead to the loss of its support function [38]. This leads to the aging of ELN-rich organs and tissues and destroys the physical barrier of tumor cell metastasis [43,44]. Moreover, the abnormal expression of elastase and the biological process triggered by elastic factors may support the development and progression of various pathological conditions. The relationships between ELN and tumor development, the role of different types of fibroblasts, and their interaction with ELN are all unresolved issues. Our study, for the first time, proposes the possibility of using ELN to predict the metastasis and prognosis of GC. This also suggests that future research should pay more attention to the relationship between fibroblasts in the TME and ELN, and this study may aid in the development of directed therapies to treat pathologies related to ELN degradation.

There are limitations to our study. For instance, the analysis of mRNA markers and molecular functional prediction in tumors are derived from transcriptome sequencing databases; therefore, although this study included the public dataset TCGA and our research center dataset, the results should be interpreted with caution. Considering the tumor stroma, different parts often reflect different pathological characteristics. TMAs were used in this study, and it is likely that they cannot fully reflect the characteristics of all TMEs due to the small sampling site. In particular, part of the invasive front and tumor center are not fully considered.

In conclusion, the current study demonstrates the prognostic importance of ELN protein expression both as a single marker and combined with lymph node metastasis rate analysis. Future studies should assess larger patient cohorts to determine the clinical utility

A

Characteristics	Number of patients	HR (95% CI)	P value
ELN expression			<0.001
High	38	Reference	
Low	62	0.254 (0.118–0.545)	<0.001
Sex			0.712
Female	28	Reference	
Male	72	1.175 (0.499–2.765)	0.712
Age	100	0.992 (0.957–1.028)	0.646
BMI	100	0.938 (0.842–1.044)	0.238
Tumor infiltration pattern			0.598
INFc	48	Reference	
INFb	16	0.843 (0.280–2.541)	0.761
INFa	20	0.566 (0.188–1.708)	0.313
Lymphatic infiltration			0.872
Positive	45	Reference	
Negative	55	1.064 (0.503–2.249)	0.872
Venous infiltration			0.255
Positive	30	Reference	
Negative	70	1.689 (0.685–4.166)	0.255
Nerve infiltration			0.135
Positive	75	Reference	
Negative	25	0.446 (0.155–1.286)	0.135
T stage			0.39
T4	38	Reference	
T3	45	0.591 (0.268–1.302)	0.192
T2	13	0.348 (0.079–1.533)	0.163
T1	4	0.585 (0.077–4.452)	0.605
Lymph node metastasis rate	100	14.051 (3.347–58.990)	<0.001
Tumor location			0.385
Lower third	54	Reference	
Middle and Upper third	42	0.571 (0.256–1.271)	0.17
Entire stomach	4	0.706 (0.094–5.295)	0.735
Lauren classification	100		0.995
diffuse	31	Reference	
intestinal	35	1.035 (0.421–2.549)	0.94
mixed	19	0.899 (0.301–2.685)	0.849
unknow	15	0.947 (0.291–3.077)	0.928
HER2 expression			0.339
Negative	82	Reference	
Positive	18	1.554 (0.629–3.836)	0.339
CEA			0.896
≤5 ng/ml	86	Reference	
>5 ng/ml	14	1.073 (0.372–3.094)	0.896
CA-199			0.667
≤37 U/ml	88	Reference	
>37 U/ml	12	0.769 (0.232–2.546)	0.667
CA724			0.06
≤6 U/ml	74	Reference	
>6 U/ml	26	2.073 (0.970–4.429)	0.06

B

Characteristics	N	HR (95% CI)	P value
Group			
ELN High expression	38		
ELN Low expression	62	0.370 (0.140–0.982)	0.046
N stage			
N2	24		
N3	31	4.698 (1.339–16.483)	0.016
N1	19	2.088 (0.393–11.092)	0.388
N0	26	2.321 (0.525–10.249)	0.267

C

HR = 0.28 (0.12–0.65)
Log-rank $p < 0.001$

High	36	25	17	16	16
Low	63	62	56	50	45

D

E

F

Figure 6. (A) Univariate Cox analysis of ELN protein expression and the clinicopathological variables. (B) Multivariate Cox analysis of ELN protein expression and the clinicopathological variables. (C) Kaplan–Meier survival analysis of the OS for patients with different ELN protein expression levels in TMAs. (D) Nomogram prognostic model. (E) Calibration analysis for 2 and 3 years. (F) Decision curve analysis in 2 and 3 years. HR, hazard ratio.

of using ELN as a biomarker, particularly in relation to immune cells in the TME of GC and the efficacy of immunotherapy.

Author contributions statement

TF, LZ and XY designed and conceived this project, and they contributed equally to this work. TF, XY, YW, XZ and SY interpreted and analyzed the data. YX and LZ revised the manuscript for important intellectual content. XY, TF and YW participated in the patient information collection. TF, XB, XJ and LZ performed the experiments.

Ethics approval and consent to participate

All programs followed were according to the ethical standards of the Human Subjects Responsibility Committee (institutions and countries), as well as the 1964 Helsinki Declaration and subsequent editions. This research was approved by Harbin Medical University Cancer Hospital Ethics Committee of (Approval Number: SHGC-1029). Written informed consent was obtained from all participants.

Data availability statement

The datasets used in this study are available from the corresponding author on reasonable request. More information can also be obtained from the Gastric Cancer Information Management System v1.2 of Harbin Medical University Cancer Hospital (Copyright No. 2013SR087424, http://www.sgihmu.com/). The datasets for the HMU-training cohort and HMU-validation cohorts presented in this study can be found in online repositories (GSE184336 and GSE179252).

References

1. Siegel RL, Miller KD, Fuchs HE, *et al*. Cancer statistics, 2022. *CA Cancer J Clin* 2022; **72**: 7–33.
2. Islam Khan MZ, Tam SY, Law HKW. Advances in high through-put proteomics profiling in establishing potential biomarkers for gastrointestinal cancer. *Cell* 2022; **11**: 973.
3. Chiarello MM, Fico V, Pepe G, *et al*. Early gastric cancer: a challenge in Western countries. *World J Gastroenterol* 2022; **28**: 693–703.
4. Fang T, Wang Y, Yin X, *et al*. Diagnostic sensitivity of NLR and PLR in early diagnosis of gastric cancer. *J Immunol Res* 2020; **2020**: 9146042.
5. Kole C, Charalampakis N, Vailas M, *et al*. Immunotherapy for gastroenteropancreatic neuroendocrine neoplasms (GEP-NENs): a 2021 update. *Cancer Immunol Immunother* 2022; **71**: 761–768.
6. Oh SE, An JY, Choi MG, *et al*. Comparisons of remnant primary, residual, and recurrent gastric cancer and applicability of the 8th AJCC TNM classification for remnant gastric cancer staging. *Eur J Surg Oncol* 2020; **46**: 2236–2242.
7. Sexton RE, Al Hallak MN, Diab M, *et al*. Gastric cancer: a comprehensive review of current and future treatment strategies. *Cancer Metastasis Rev* 2020; **39**: 1179–1203.
8. Kinoshita J, Yamaguchi T, Moriyama H, *et al*. Current status of conversion surgery for stage IV gastric cancer. *Surg Today* 2021; **51**: 1736–1754.
9. Kakeji Y, Maehara Y, Sumiyoshi Y, *et al*. Angiogenesis as a target for gastric cancer. *Surgery* 2002; **131**: S48–S54.
10. Fang T, Yin X, Wang Y, *et al*. Proposed models for prediction of mortality in stage-I and stage-II gastric cancer and 5 years after radical gastrectomy. *J Oncol* 2022; **2022**: 4510000.
11. Chiu KJ, Chiou HC, Huang CH, *et al*. Natural compounds targeting cancer-associated fibroblasts against digestive system tumor progression: therapeutic insights. *Biomedicine* 2022; **10**: 713.
12. Suzuki H, Kaneko MK, Kato Y. Roles of podoplanin in malignant progression of tumor. *Cell* 2022; **11**: 575.
13. Elmentaite R, Domínguez Conde C, Yang L, *et al*. Single-cell atlases: shared and tissue-specific cell types across human organs. *Nat Rev Genet* 2022; **23**: 395–410.
14. Machla F, Angelopoulos I, Epple M, *et al*. Biomolecule-mediated therapeutics of the dentin-pulp complex: a systematic review. *Biomolecules* 2022; **12**: 285.
15. Lepucki A, Orlińska K, Mielczarek-Palacz A, *et al*. The role of extracellular matrix proteins in breast cancer. *J Clin Med* 2022; **11**: 1250.
16. Takahashi M, Kobayashi H, Mizutani Y, *et al*. Roles of the mesenchymal stromal/stem cell marker Meflin/Islr in cancer fibrosis. *Front Cell Dev Biol* 2021; **9**: 749924.
17. Di Martino JS, Nobre AR, Mondal C, *et al*. A tumor-derived type III collagen-rich ECM niche regulates tumor cell dormancy. *Nat Cancer* 2022; **3**: 90–107.
18. Lei G, Yang H, Hong T, *et al*. Elastic staining on paraffin-embedded slides of pT3N0M0 gastric cancer tissue. *J Vis Exp* 2019; **147**: e58278.
19. Gilardi L, Airò Farulla LS, Demirci E, *et al*. Imaging cancer-associated fibroblasts (CAFs) with FAPi PET. *Biomedicine* 2022; **10**: 523.
20. Boussadia Z, Gambardella AR, Mattei F, *et al*. Acidic and hypoxic microenvironment in melanoma: impact of tumour exosomes on disease progression. *Cell* 2021; **10**: 3311.

21. Schmelzer CEH, Duca L. Elastic fibers: formation, function, and fate during aging and disease. *FEBS J* 2022; **289**: 3704–3730.

22. Kalluri R. The biology and function of fibroblasts in cancer. *Nat Rev Cancer* 2016; **16**: 582–598.

23. Kalluri R, Zeisberg M. Fibroblasts in cancer. *Nat Rev Cancer* 2006; **6**: 392–401.

24. Kwa MQ, Herum KM, Brakebusch C. Cancer-associated fibroblasts: how do they contribute to metastasis? *Clin Exp Metastasis* 2019; **36**: 71–86.

25. Han C, Liu T, Yin R. Biomarkers for cancer-associated fibroblasts. *Biomark Res* 2020; **8**: 64.

26. Antonicelli F, Bellon G, Debelle L, *et al*. Elastin-elastases and inflamm-aging. *Curr Top Dev Biol* 2007; **79**: 99–155.

27. Debelle L, Tamburro AM. Elastin: molecular description and function. *Int J Biochem Cell Biol* 1999; **31**: 261–272.

28. Powell JT, Vine N, Crossman M. On the accumulation of D-aspartate in elastin and other proteins of the ageing aorta. *Atherosclerosis* 1992; **97**: 201–208.

29. Shapiro SD, Endicott SK, Province MA, *et al*. Marked longevity of human lung parenchymal elastic fibers deduced from prevalence of D-aspartate and nuclear weapons-related radiocarbon. *J Clin Invest* 1991; **87**: 1828–1834.

30. Heinz A. Elastic fibers during aging and disease. *Ageing Res Rev* 2021; **66**: 101255.

31. Heinz A. Elastases and elastokines: elastin degradation and its significance in health and disease. *Crit Rev Biochem Mol Biol* 2020; **55**: 252–273.

32. Romaniello F, Mazzaglia D, Pellegrino A, *et al*. Aortopathy in Marfan syndrome: an update. *Cardiovasc Pathol* 2014; **23**: 261–266.

33. Debret R, Le Naour RR, Sallenave JM, *et al*. Elastin fragments induce IL-1beta upregulation via NF-kappaB pathway in melanoma cells. *J Invest Dermatol* 2006; **126**: 1860–1868.

34. de Castro Bras LE, Frangogiannis NG. Extracellular matrix-derived peptides in tissue remodeling and fibrosis. *Matrix Biol* 2020; **91–92**: 176–187.

35. Ligorio M, Sil S, Malagon-Lopez J, *et al*. Stromal microenvironment shapes the intratumoral architecture of pancreatic cancer. *Cell* 2019; **178**: 160–175.e27.

36. Brassart B, Fuchs P, Huet E, *et al*. Conformational dependence of collagenase (matrix metalloproteinase-1) up-regulation by elastin peptides in cultured fibroblasts. *J Biol Chem* 2001; **276**: 5222–5227.

37. Nackman GB, Karkowski FJ, Halpern VJ, *et al*. Elastin degradation products induce adventitial angiogenesis in the Anidjar/Dobrin rat aneurysm model. *Surgery* 1997; **122**: 39–44.

38. Robinet A, Fahem A, Cauchard JH, *et al*. Elastin-derived peptides enhance angiogenesis by promoting endothelial cell migration and tubulogenesis through upregulation of MT1-MMP. *J Cell Sci* 2005; **118**: 343–356.

39. Gunda V, Verma RK, Sudhakar YA. Inhibition of elastin peptide-mediated angiogenic signaling mechanism(s) in choroidal endothelial cells by the α6(IV)NC1 collagen fragment. *Invest Ophthalmol Vis Sci* 2013; **54**: 7828–7835.

40. Yin X, Fang T, Wang Y, *et al*. Prognostic significance of serum inflammation indexes in different Lauren classification of gastric cancer. *Cancer Med* 2021; **10**: 1103–1119.

41. Cox TR. The matrix in cancer. *Nat Rev Cancer* 2021; **21**: 217–238.

42. Theocharis AD, Skandalis SS, Gialeli C, *et al*. Extracellular matrix structure. *Adv Drug Deliv Rev* 2016; **97**: 4–27.

43. Wang Y, Song EC, Resnick MB. Elastin in the tumor microenvironment. *Adv Exp Med Biol* 2020; **1272**: 1–16.

44. Lapis K, Timar J. Role of elastin-matrix interactions in tumor progression. *Semin Cancer Biol* 2002; **12**: 209–217.

SUPPLEMENTARY MATERIAL ONLINE

Table S1. The clinicopathological characteristics of 6 distant and 36 non-distant metastases

Table S2. The relationship between ELN expression in paracancerous tumor tissue and clinicopathological features

Table S3. The relationship between VIM expression in cancer tissues and clinicopathological characteristics